

Dynamic topography of the ice-covered Arctic Ocean from ICESat

R. Kwok¹ and J. Morison²

Received 2 November 2010; revised 3 December 2010; accepted 22 December 2010; published 26 January 2011.

[1] We construct the dynamic ocean topography (DOT) of the Arctic Ocean, for five ICESat campaigns (winter of 2004–2008), using sea surface height estimates in open leads. Results show that the mean winter DOT over the Arctic Ocean varies by ~ 1 m and features a distinct dome of ~ 40 cm over the Beaufort Sea. Standard deviation of the mean field is ~ 20 cm. Spatial coherence between the five winter DOTs is consistently high (>0.9), whereas the coherence between the DOTs and the winter (DJFM) sea-level pressure fields over the Arctic Basin is variable. This suggests persistence of the underlying hydrodynamic processes at interannual time-scales compared to seasonal atmospheric forcing. Comparison of dynamic heights (DH) from hydrographic surveys and the DOT in 2008 shows a remarkable correlation of 0.92. The geostrophic velocity fields computed from the DOT and interpolated DH fields highlight the smaller scale oceanographic features in the satellite estimates. **Citation:** Kwok, R., and J. Morison (2011), Dynamic topography of the ice-covered Arctic Ocean from ICESat, *Geophys. Res. Lett.*, 38, L02501, doi:10.1029/2010GL046063.

1. Introduction

[2] The dynamic ocean topography (DOT) is the deviation of the sea surface from the height of the geoid. Horizontal gradients in the DOT determine the surface geostrophic circulation. Prior to the era of satellite altimetry, oceanographers have inferred variations in DOT from hydrographic measurements by integrating the specific volume from the surface to an assumed level of no motion. Gradients in the resulting dynamic heights (DH) relative to the level of no motion yield the velocity profile due to density gradients. Since the true velocity at the level of no motion is not known, the barotropic current associated with, for example the direct set up of the sea surface by wind forcing, is not known. Satellite altimetry derived estimates of DOT in ice-free oceans have provided the absolute DOT needed to register absolute velocity.

[3] In the past, sea surface height (SSH) measurements of high latitude oceans are limited by the number of polar-orbiting altimeters, and restricted to regions with large expanses of open-ocean during the melt season. *Peacock and Laxon* [2004] were the first to extract the SSH of the ice-covered seas from ERS-2 data using radar echoes from open leads, and the first to produce a map of SSH variability of the Arctic Ocean between 60°N and 81.5°N .

[4] With the launch of ICESat in 2003, higher resolution (50–70 m) and higher precision (shot-to-shot repeatability

of ~ 2 – 3 cm) elevation profiles of the sea ice cover from the lidar have allowed the unambiguous identification of new openings (of water or thin ice) and thus improved SSH estimates over the Arctic Ocean [Kwok *et al.*, 2004]. With its higher inclination orbit (94°), ICESat also covered a larger fraction of the Arctic Ocean than previous altimeter missions. Recent work by *Forsberg et al.* [2006] provided an initial assessment of a multi-year mean DOT of the Arctic Ocean using combined estimates of SSH from ERS and ICESat SSH; they found reasonable agreement between satellite-derived and model estimates.

[5] The ICESat mission ended in 2010. Retrieval of SSH in ICESat data has become more mature since its launch [Kwok *et al.*, 2007; Kwok and Cunningham, 2008]. In this note, we provide a more in-depth examination of the DOT of the Arctic Ocean using SSH estimates from five winter campaigns (2004–2008). In particular, we compare the 2008 DOT with the DH estimates from hydrographic measurements.

2. Data Description

2.1. ICESat Sea Surface Height and DOT

[6] ICESat elevation data from five winter campaigns (2004–2008) are used in this note. Coverage of the altimeter data is up to 86°N . Data products are of Release 431: the latest available in terms of quality and precision at the time of this writing. The length of each winter campaign is ~ 34 days, and typically starts around mid-February. Inter-campaign biases in elevation, due mostly to saturation issues associated with varying received laser energies, were estimated by a comprehensive analysis of all crossover elevation differences at Lake Vostok, Antarctica (provided by C. Shuman, unpublished data, 2010). These biases have been removed. Because the relative biases are proportional to the magnitude of received laser energies, the biases are generally moderate because of the lower received energies from the sea surface. For relatively level surfaces, the expected uncertainty of individual absolute elevation estimates after the removal of the biases is ~ 15 cm.

[7] We compute the DOT (h_d) as the difference between the height of the sea surface (h) and that of the EGM2008 geoid – both measured relative to the WGS84 ellipsoid [Pavlis *et al.*, 2008]: $h_d = h - h_{\text{geoid}}$ (Figure 1a). Here, h is the elevation of the sea surface from ICESat after removal of tides (ocean, load, and solid earth) and the inverted barometer effect [Kwok *et al.*, 2006]. Figure 1b shows the mean DOT from the five winter campaigns (discussed in the next section). Since a large fraction of the Arctic Ocean is covered by sea ice for most of the year, observations of the sea surface are available only where open water is exposed along occasional cracks in the ice cover (leads). As leads are finite in width (typically less than ~ 100 m), the spatial resolution of the ICESat lidar (50–70 m) limits the number

¹Jet Propulsion Laboratory, California Institute of Technology, Pasadena, California, USA.

²Polar Science Center, University of Washington, Seattle, Washington, USA.

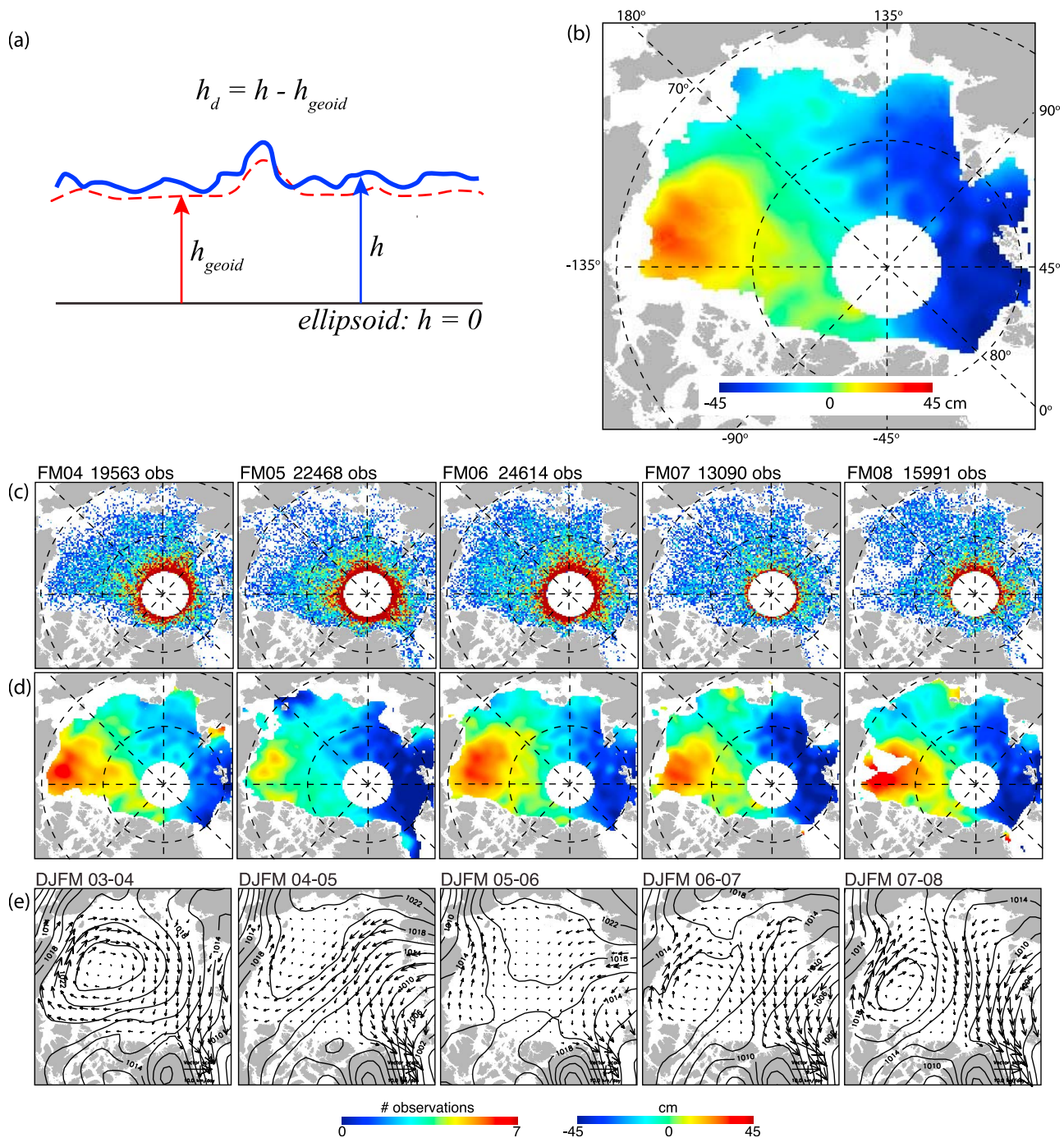


Figure 1. Dynamic ocean topography (DOT) of the Arctic Ocean from ICESat. (a) Geometric relationships between DOT, sea surface height, geoid, and reference ellipsoid. (b) Mean DOT of the Arctic Ocean from five winter ICESat campaigns (2004–2008) using estimates of sea surface height in open leads. (c) Spatial density (counts) of sea surface estimates within 25 km by 25 km grids used in the construction. (d) DOT for the five winter ICESat campaigns (2004–2008). (e) Mean DJFM (December through March) sea-level pressure and ice motion of the five winters. (contour interval: 4 hPa)

of available sea surface observations. Ice/water classification procedures [Kwok *et al.*, 2007] are used to identify the set of sea surface samples that are of interest in the present analysis. The ice returns are not used.

2.2. Hydrographic Data

[8] The North Pole Environmental Observatory (NPEO) airborne hydrographic survey (Figure 2) in March–April

2008 has been discussed by McPhee *et al.* [2009] and Alkire *et al.* [2010]. It included 35 stations made by landing an aircraft on the sea ice in the Beaufort Sea (15) and North Pole region (20) and measuring ocean temperature and salinity profiles to 800 m depth with a Conductivity-Temperature-Depth (CTD) instrument and recovering water samples for chemical analysis. An additional eight stations were made in the Beaufort Sea using Airdropped eXpendable

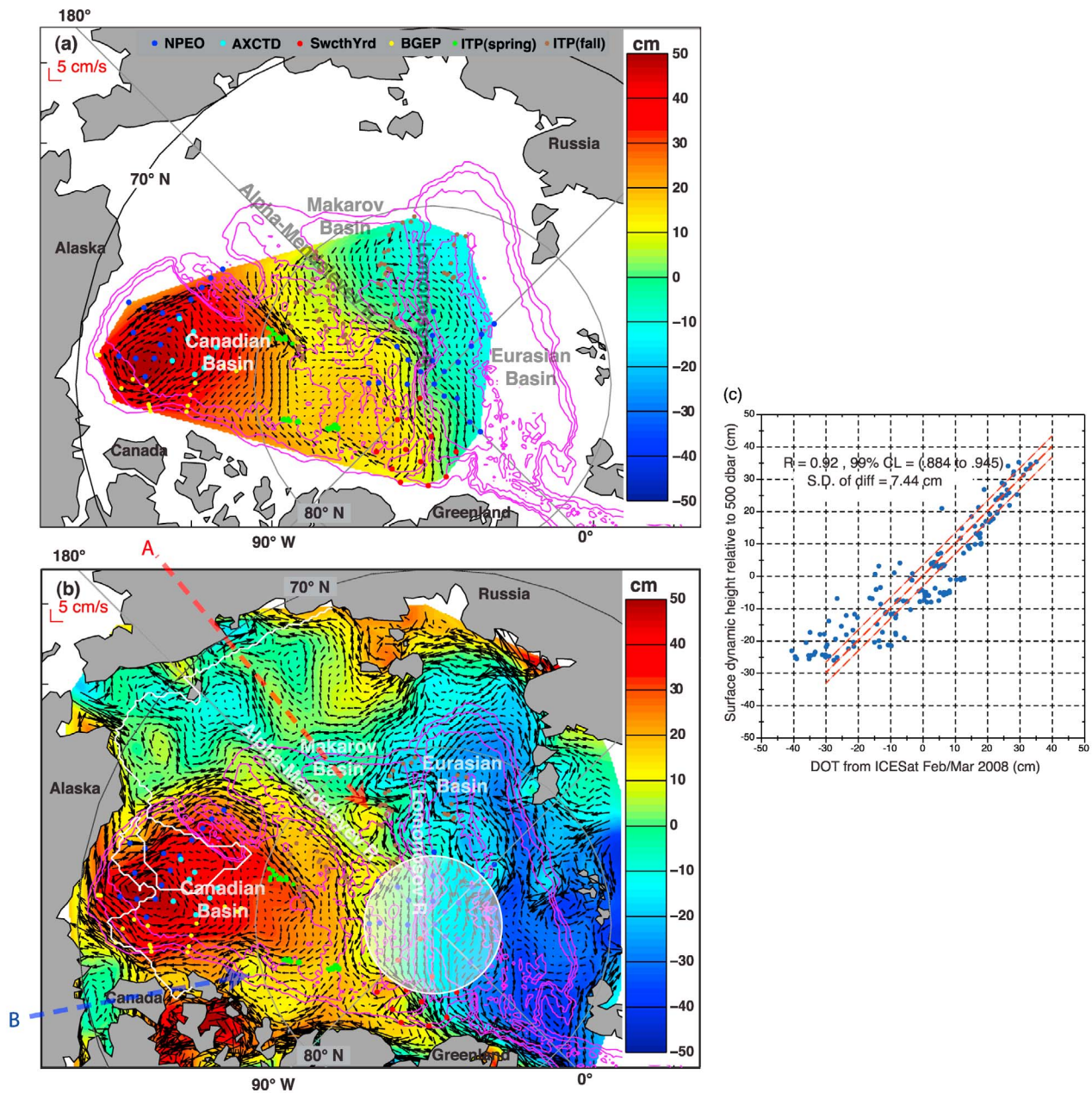


Figure 2. (a) Arctic Ocean dynamic height from 2008 hydrography-derived DH relative to 500 dbar. Data sources as explained in the text are given according to the color of the station dots. (b) DOT ICESat altimetry in 2008. The white shaded circle is the region not covered by ICESat and the DOT is wholly interpolated. The area shoreward of the white line in the Canadian Basin is interpolated from sparse DOT observations due to an absence of lead returns. (c) DH from hydrography versus DOT from ICESat at the 2008 hydrographic stations, correlation coefficient = 0.92.

CTDs (AXCTD) in April 2008. These data were supplemented with CTD stations made by the Switchyard program in the Lincoln Sea (11 stations in May 2008) and CTD data from nine automated Ice Tethered Profiler (ITP) buoys (<http://www.whoi.edu/page.do?pid=20756>). Data from the buoys were limited to January to June 2008 (44 Spring ITP 10-day averages) except 3 Fall ITP buoys from the southern part of the Makarov Basin from September through December 2008 (64 Fall ITP 10-day averages). To resolve the structure in the easternmost part of the Beaufort Sea, we

used CTD stations made by the Beaufort Gyre Exploration Project (BGEP) in September and October of 2007 (yellow points in Figure 2). These were corrected to springtime profiles with a seasonal correction mainly in the upper 100-m of the water column derived by taking the differences in salinity and temperature profiles at the closest locations sampled by NPEO in Spring 2008 and by BGEP in Fall 2007. These difference profiles were then added to the Fall 2007 profiles to yield proxy springtime profiles. Dynamic heights, the integral of specific volume between pressure

Table 1. Cross-Correlations and Standard Deviation of the Differences, in cm, Among the Dynamic Topography of the Five Winter Campaigns and Their Correlations With the DJFM Sea-Level Pressure Fields^a

	SD	2004	2005	2006	2007	2008	Mean	Sea Level Pressure
2004	18.9	1.00	0.93	0.95	0.93	0.92	0.96	0.51
			6.7	6.5	8.9	9.1	5.3	
2005	18.9		1.00	0.96	0.94	0.92	0.97	0.66
				5.6	7.7	9.1	4.5	
2006	20.2			1.00	0.96	0.95	0.99	0.03
					6.1	7.2	3.2	
2007	21.9				1.00	0.95	0.99	0.78
						6.7	4.4	
2008	21.8					1.00	0.98	0.82
							5.5	
Mean	19.6						1.00	0.74

^aSecond column shows the standard deviation of the individual fields.

surfaces, relative to 500 dbar were computed for each station, and the gradients in DH were used to estimate surface geostrophic currents relative to the 500 dbar level.

3. Dynamic Ocean Topography From ICESat

[9] Figure 1c shows the spatial density and number of sea surface returns used in the construction of the five winter DOT fields (Figure 1d). The spatial density is determined by the availability of open leads, as mentioned above, as well as the convergence of the satellite tracks near the poleward limits of the altimeter orbit. Clearly, the number of observations increases with latitude. Gaps in the DOT over the Beaufort Sea in 2008 are due to the low density of leads found in the ICESat data during that campaign. Sea surface estimates at individual ICESat spots (~50–70 m) are convolved with a 100-km Gaussian-kernel to obtain the smoothed fields in Figure 1d. Smoothing serves to reduce the noise of the sea surface measurements and the contribution of residual geoid errors at length scales below the width of the kernel.

[10] The mean field (Figure 1b) is an average of the five winter DOT fields. Broadly, the spatial pattern of the mean winter DOT of the Arctic Ocean (Figure 1) varies by ~1 m and features a distinct dome of ~40 cm over the Beaufort Sea with a gradual down slope across the Arctic Ocean towards the Barents Sea. The standard deviation of the mean field is ~20 cm.

[11] The large-scale spatial pattern of the five winter DOTs certainly exhibit similar features. To measure their similarity, we compare the standard deviation of the fields, and calculate the cross-correlation and differences between the fields (see Table 1). The standard deviations of individual fields range from 19 to 22 cm, while the differences, at only 5 to 9 cm, are a fraction of the overall variability. The Beaufort Sea dome of the 2005 DOT stands out as being lower than the other winter fields.

[12] In 2006 the region of elevated DOT (Figure 1d, center) expanded to an anticyclonic extreme at 145° W, aligning the geostrophic transpolar drift in the ocean with the Lomonosov Ridge. This is broadly consistent with the shift in orientation of transpolar drift from 2000 to 2006 estimated on the basis of surface freshening in the North Pole region [Morison *et al.*, 2006] and trends in ocean bottom pressure [Morison *et al.*, 2007].

[13] Spatial coherence between the five winter DOTs is consistently high (>0.9) and the mean field explains more

than 90% of the variability of the individual fields. These results suggest that interannual variability in the winter DOT is small relative to the mean pattern and the persistence of the underlying hydrodynamic processes that sustain the sea surface topography.

[14] In a steady state situation, we expect DOT to correlate spatially with NCEP/NCAR sea-level pressure (SLP), with domes (troughs) under highs (lows) in SLP (an indicator of the geostrophic atmospheric circulation) because of adjustment of the ocean circulation to Ekman convergence (divergence) associated with negative (positive) wind stress curl. To see how close Arctic Ocean DOT and SLP come to the steady state ideal, we compute annual point-to-point cross-correlation between the winter DOTs and the (December–March DJFM) SLP distributions. We chose the four-month DJFM average because we expect the ocean response to be more of an expression of the average winter SLP distribution than just the short-term February–March distributions. Results (Table 1) show that seasonal coherence between the DOTs and the winter (DJFM) sea-level pressure fields over the Arctic Basin average 0.56 but are highly variable year-to-year, ranging from 0.03 to 0.82. The 5-year mean SLP field, however, explains ~55% (correlation coefficient = 0.74) of the mean DOT field suggesting ocean adjustment to the atmospheric forcing at longer time-scales.

[15] Besides the large-scale spatial and temporal variability, there are persistent small-scale (200–500 km) features that are prominent in the DOTs. One example is the high DOT over the Northwind Rise (~76°N, 160°E) and associated northward flow over the Chukchi Cap (~76°N, 165°W), which appear almost every year as a sometimes-dominant (e.g., 2006, 2008) western branch of the Beaufort Gyre. Another is the 100–200 km relative depression in DOT north of Prince Patrick Is. (~79°N, 117° W) seemingly associated with an eastward broadening of the continental shelf in that region. These regional circulation patterns associated with bathymetric structures persist in some form, but vary with annual variations in the larger-scale circulation.

4. Comparison of DOT With Dynamic Height Field (2008)

[16] The surface DH relative to 500 dbar and the corresponding velocities (Figure 2a) from the 2008 hydrographic data show a doming of up to 50 cm and characteristic anticyclonic circulation in the Beaufort Sea. The pattern is

most intense in the southern third of the Canadian Basin, with an intense westward flow at 72°N along the continental slope to cross the Northwind Rise (~75°N, 155°W) and a tight eastward return flow at 75°N. There is also a strong northward flow along the margin between the Northwind Abyssal Plain (~77°N, 160°W) and Chukchi Cap (~79°N, 165°W), and division north of the Northwind Rise into a southwestward flow and a west-to-east stream along 80°N. However, the gyre as a whole extends to a significant degree to fill the whole Canadian Basin, with an additional west-to-east velocity stream along the Alpha-Mendeleev ridges.

[17] In 2008, the main front in surface DH, which defines the upper ocean contribution to the Transpolar Drift, is aligned with the Alpha-Mendeleev Ridge system. This is virtually the same pattern found in 1993 [Morison *et al.*, 1998] at the heart of the 1990s cyclonic circulation pattern. It contrasts with the anticyclonic pattern characterizing pre-1990s climatology [EWG, 1997], in which the front and Transpolar Drift are lined up with the Lomonosov Ridge (~ along 135°E and 45°W).

[18] On the Eurasian side of the front, the DH and velocities of Figure 2a suggest a cyclonic pattern sweeping eastward across the Makarov Basin and Mendeleev Ridge region (~82°N, 180°) and feeding the two northern branches (80°N and Alpha Mendeleev Ridge) of Canadian Basin eastward circulation.

[19] The February–March 2008 DOT and circulation from ICESat (Figure 2b) largely matches the hydrography-determined pattern (Figure 2a). The only adjustment in this comparison has been to recognize that the DH from hydrography are not absolute and so to shift all values of DH by the same constant so that the average of DH at the hydrographic stations matches the average of DOT at the hydrographic stations. The correlation between variations in DOT and surface DH relative to 500 dbar at the hydrographic stations (Figure 2c) is 0.92 (0.88 to 0.95 for 99% confidence limits). The standard deviation of the difference between DOT and the DH is 7.4 cm over a range of 80 cm.

[20] The main features of the DH (Figure 2a) and DOT (Figure 2b) are the same. As with the hydrography-determined pattern, the DOT rendition of the Beaufort Gyre is most intense (40+ cm peak in the dome) in the southern Canadian Basin but extends to the Alpha-Mendeleev Ridge system. The main differences in the Canadian Basin are likely due to the improved spatial coverage and resolution of the ICESat DOT. The southwestward return flow from 80–75°N, 140°W in Figure 2a is not distinct in Figure 2b, and appears to be partly an artifact of interpolation between distant hydrographic stations. Similarly, though the Mendeleev and 80°N eastward return streams appear in the DOT-derived pattern, they are less distinct than in these data sparse regions of the hydrography. The exception is the hole in ICESat coverage around the Pole indicated by the white shaded circle in Figure 2b. DOT is interpolated across this circle and the height gradients and velocities consequently are unnaturally linear compared to the hydrography-derived heights and velocity fields near the Pole. The alignment of the main front in DOT, like the DH of Figure 2a, is aligned with the Alpha-Mendeleev Ridge system, supporting the idea that the 2008 circulation pattern was cyclonic, similar to the mid 1990s.

[21] The most obvious advantage of ICESat DOT is data coverage, which includes the Russian shelves and major

portions of the Eurasian and Makarov basins, areas critical to understanding Arctic Ocean circulation. In 2008, this dog-leg-shaped region extends through east longitudes roughly paralleling the Russian continental slope. It is characterized by a semi-continuous trough of low DOT made up of several segmented cells of cyclonic circulation. The pattern carries shelf water, freshened by Russian river runoff eastward along the Russian coast. The Eurasian Basin cell carries some shelf water around to the Eurasian side of the Transpolar Drift. However the branches nearest the Russian coast continue east across the shelf to the cyclonic cell in the Makarov Basin and around a cyclonic cell in the East Siberian – Chukchi seas (~72°N, 180°) to feed the Beaufort Sea across the Mendeleev Ridge and Chukchi Cap.

[22] The DOT circulation pattern (Figure 2b) also reveals smaller-scale features that are only hinted at by hydrography. As mentioned above (Figure 1b), DOT is characterized by a semi-permanent, 100km anticyclonic dome (83°N, 167°E, arrow A, Figure 2b) in the middle of a larger-scale cyclonic pattern in the Makarov Basin. This is about 100 km east of the center of a smaller anticyclonic feature picked up in hydrographic data from two ITP buoys (Figure 2a). This feature is nearly over a small seamount at the end of the Oden Spur off the Lomonosov Ridge [Jakobsson *et al.*, 2004], suggesting the presence of a Taylor column. The cyclonic feature in DOT at 79°N, 125°W (arrow B, Figure 2b) is similarly energetic and of similar size. It also seems to be persistently associated with a bathymetric feature, a wide segment in the continental shelf and with a poorly resolved weaker cyclonic bend in the DH circulation (Figure 2a). The wide spot in the shelf is punctuated by at least one deep canyon, but we can only speculate that this cyclonic circulation is connected with conservation of vorticity over this relative bathymetric depression.

5. Conclusions

[23] In this note, we examined the DOT of the ice-covered Arctic Ocean constructed with SSH estimates from five winter ICESat campaigns (2004–2008), and compared the results with DH computed from hydrographic surveys. The high-resolution lidar allows the identification of sea surface height in narrow leads. The mean winter DOT varies by ~1 m over the Arctic Ocean and features a distinct dome of ~40 cm over the Beaufort Sea. High spatial coherence (>0.9) between the five winter DOTs suggests persistence and dominance of the underlying hydrodynamic processes at interannual time scales compared to seasonal atmospheric forcing.

[24] The agreement between ICESat-derived DOT and DH from 2008 hydrography (Figure 2) gives us confidence in the DOT derivations and emphasizes the importance of the baroclinic component of Arctic Ocean circulation. The basic pattern of high DOT on the Pacific side of the basin (particularly the Beaufort Gyre) and low DOT on the Atlantic side (Figure 1) is in agreement with climatology, but the ~80 cm contrast between the Beaufort Gyre and Fram Strait DOT (Figure 1) is twice as great as the difference in DH from 1950–2000 climatology [Steele and Ermold, 2007], suggesting enhanced freshwater content on the Pacific side [e.g., McPhee *et al.*, 2009]. Between 2004 and 2008, the orientation of oceanic Transpolar Drift determined by the orientation of the gradient in DOT (Figure 2) is variable, but in 2008 is aligned with the Alpha-

Mendeleyev Ridge system (Figure 2). This suggests a cyclonic circulation pattern reminiscent of the 1990s [Morison *et al.*, 1998]. The circulation in the Eurasian Basin associated with this pattern is conducive to transport of Russian river water eastward to the Canadian Basin [Steele and Boyd, 1998], which would explain at least in part freshening there [e.g., Proshutinsky *et al.*, 2009; McPhee *et al.*, 2009].

[25] **Acknowledgments.** The authors also wish to thank Matt Alkire, Miles McPhee, Roger Andersen, Glenn Cunningham, Cecilia Peralta-Ferriz, Andrey Proshutinsky, Ignatius Rigor, Mike Steele, and John Toole. R.K. performed this work at the Jet Propulsion Laboratory, California Institute of Technology, under contract with NASA. J.M. performed this work under NSF grants OPP 0352754, ARC-0634226, ARC-0856330, and NASA grant NNX08AH62G.

References

- Alkire, M., K. Falkner, J. Morison, R. Collier, C. Guay, R. Desiderio, I. Rigor, and M. McPhee (2010), Sensor-based profiles of the NO parameter in the central Arctic and southern Canada Basin: New insights regarding the cold halocline, *Deep Sea Res., Part I*, *57*, 1432–1443, doi:10.1016/j.dsr.2010.07.011.
- Environmental Working Group (EWG) (1997), *Joint U.S.-Russian Atlas of the Arctic Ocean, Oceanography Atlas for the Winter Period*, National Ocean Data Center, CD-ROM available from NODC.
- Forsberg, R., et al. (2006), Arctic Ocean geoid, ice thickness, and mean sea level - The ARCGICE project, paper presented at 15 Years of Progress in Radar Altimetry Symposium, Eur. Space Agency, Venice, Italy.
- Jakobsson, M., R. Macnab, N. Cherkis, and H. Schenke (2004), The International Bathymetric Chart of the Arctic Ocean (IBCAO), *Res. Publ. RP-2*, National Geophysical Data Center, Boulder, Colorado, USA.
- Kwok, R., and G. F. Cunningham (2008), ICESat over Arctic sea ice: Estimation of snow depth and ice thickness, *J. Geophys. Res.*, *113*, C08010, doi:10.1029/2008JC004753.
- Kwok, R., H. J. Zwally, and D. Yi (2004), ICESat observations of Arctic sea ice: A first look, *Geophys. Res. Lett.*, *31*, L16401, doi:10.1029/2004GL020309.
- Kwok, R., G. F. Cunningham, H. J. Zwally, and D. Yi (2006), ICESat over Arctic sea ice: Interpretation of altimetric and reflectivity profiles, *J. Geophys. Res.*, *111*, C06006, doi:10.1029/2005JC003175.
- Kwok, R., G. F. Cunningham, H. J. Zwally, and D. Yi (2007), Ice, Cloud, and land Elevation Satellite (ICESat) over Arctic sea ice: Retrieval of freeboard, *J. Geophys. Res.*, *112*, C12013, doi:10.1029/2006JC003978.
- McPhee, M. G., A. Proshutinsky, J. H. Morison, M. Steele, and M. B. Alkire (2009), Rapid change in freshwater content of the Arctic Ocean, *Geophys. Res. Lett.*, *36*, L10602, doi:10.1029/2009GL037525.
- Morison, J. H., M. Steele, and R. Andersen (1998), Hydrography of the upper Arctic Ocean measured from the nuclear submarine *USS Pargo*, *Deep Sea Res., Part I*, *45*, 15–38, doi:10.1016/S0967-0637(97)00025-3.
- Morison, J., M. Steele, T. Kikuchi, K. Falkner, and W. Smethie (2006), Relaxation of central Arctic Ocean hydrography to pre-1990s climatology, *Geophys. Res. Lett.*, *33*, L17604, doi:10.1029/2006GL026826.
- Morison, J., J. Wahr, R. Kwok, and C. Peralta-Ferriz (2007), Recent trends in Arctic Ocean mass distribution revealed by GRACE, *Geophys. Res. Lett.*, *34*, L07602, doi:10.1029/2006GL029016.
- Pavlis, N. K., S. Holmes, S. Kenyon, and J. K. Factor (2008), An Earth gravitational model to degree 2160, *Geophys. Res. Abstr.*, *10*, A-01891.
- Peacock, N. R., and S. W. Laxon (2004), Sea surface height determination in the Arctic Ocean from ERS altimetry, *J. Geophys. Res.*, *109*, C07001, doi:10.1029/2001JC001026.
- Proshutinsky, A., R. Krishfield, M.-L. Timmermans, J. Toole, E. Carmack, F. McLaughlin, S. Zimmerman, M. Itoh, and K. Shimada (2009), The Beaufort Gyre freshwater reservoir: State and variability from observations, *J. Geophys. Res.*, *114*, C00A10, doi:10.1029/2008JC005104.
- Steele, M., and T. Boyd (1998), Retreat of the cold halocline layer in the Arctic Ocean, *J. Geophys. Res.*, *103*, 10,419–10,435, doi:10.1029/98JC00580.
- Steele, M., and W. Ermold (2007), Steric sea level change in the Northern Seas, *J. Clim.*, *20*(3), 403–417, doi:10.1175/JCLI4022.1.

R. Kwok, Jet Propulsion Laboratory, California Institute of Technology, 4800 Oak Grove Dr., Pasadena, CA 91109, USA.

J. Morison, Polar Science Center, University of Washington, Seattle, WA 98105, USA.